ACS APPLIED MATERIALS & INTERFACES

Research Article

www.acsami.org

Relationship between $BaTiO_3$ Nanowire Aspect Ratio and the Dielectric Permittivity of Nanocomposites

Haixiong Tang, Zhi Zhou, and Henry A. Sodano*

Department of Materials Science and Engineering, University of Florida, Gainesville, Florida 32611, United States

ABSTRACT: The aspect ratio of barium titanate ($BaTiO_3$) nanowires is demonstrated to be successfully controlled by adjusting the temperature of the hydrothermal growth from 150 to 240 °C, corresponding to aspect ratios from 9.3 to 45.8, respectively. Polyvinylidene fluoride (PVDF) nanocomposites are formed from the various aspect ratio nanowires and the relationship between the dielectric constant of the nanocomposite and the aspect ratio of the fillers is quantified. It was found that the dielectric constant of the nanocomposite increases with the aspect ratio of the nanowires. Nanocomposites with 30 vol % $BaTiO_3$ nanowires and an aspect ratio of 45.8 can reach a dielectric constant of 44.3, which is 30.7% higher than samples with an aspect ratio of 9.3 and 352% larger than the polymer matrix. These results demonstrate that using high-aspect-ratio nanowires is an effective way to control and improve the dielectric performance of nanocomposites for future capacitor applications.

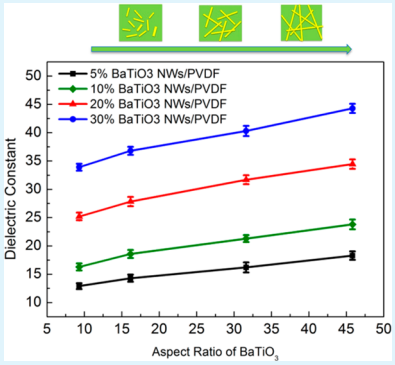

KEYWORDS: *nanowire, $BaTiO_3$, nanocomposite, dielectric, aspect ratio*

1. INTRODUCTION

High dielectric constant (κ) materials have received increased interest for various applications including energy storage, high-κ capacitors, electroactive devices and gate dielectrics.[1−3] A high-κ capacitor is one of the important components developed to allow further miniaturization of microelectronic components. Recently, nanocomposites with ferroelectric ceramic in polymer composites have been demonstrated to be one of promising material strategies for high-κ capacitors, because they can combine high dielectric permittivity from the ceramic with good mechanical strength, flexibility and ease of casting films from the polymer.[4−7] In addition, the dielectric performance of these composites can be controlled by microstructure and concentration of the fillers to meet the requirement of the various applications.[7−10]

To achieve high-κ nanocomposites, researchers have developed many approaches to improving the dielectric permittivity of the nanocomposites. For example, high dielectric permittivity fillers (PZT, $BaTiO_3$)[7,8] and high dielectric permittivity polymers such as poly(vinylidene fluoride-*co*-trifluoroethylene) (P(VDF-TrFE)), and poly(vinylidene fluoride-trifluoroethylene-chlorofluoroethylene) (P(VDF-TrFE-CFE)) have been employed to fabricate high-κ nanocomposites.[10,11] However, P(VDF-TrFE) and P(VDF-TrFE-CFE) are costly and form lossy capacitors. Also, a high volume fraction (>50 vol %) of the filler is necessary to fabricate high-κ composites. However, this method causes high mass density, low flexibility, and poor mechanical performance of the composites.[8,12]

To overcome these limitations of the nanocomposite, promising work has recently been conducted based on aspect ratio (AR) of the fillers. First, many models have shown that high-aspect-ratio fillers can improve the dielectric constant of the nanocomposites.[13−15] Our previous research has also demonstrated that high AR NWs can improve the dielectric constant of the nanocomposites more efficiently as compared to spherical particles.[8,16] This fundamental discovery has led many researches to follow this route to prepare composites with improved dielectric permittivity.[17−19] However, high AR fillers still have not been investigated as extensively as spherical fillers because of challenges in manufacturing NWs, especially for AR > 15. Here, the relationship between the AR of the filler and the dielectric constant of the nanocomposites is quantified. A novel and simple method is reported to tailor the AR of $BaTiO_3$ NWs with an AR as high as 45.8. The dielectric constant of the nanocomposites with 30 vol % and an AR of 45.8 NWs can be as high as 44.3, which is 3.5 times larger than the neat polymer. Therefore, the results and methods presented here can be widely applied to the manufacture of high-κ capacitors in the future.

2. EXPERIMENTAL SECTION

2.1. Synthesis of $BaTiO_3$ NWs with Different Aspect Ratio. The $BaTiO_3$ NWs was synthesized on the basis of a two-step hydrothermal reaction.[16,20,21] The first step in the reaction is to synthesize sodium titanate ($Na_2Ti_3O_7$) nanowires with high aspect ratio, which act as the precursor crystals for the $BaTiO_3$ NWs. First, 1.88 g of titanium dioxide (TiO_2) powder (Sigma-Aldrich, ACS certified, 99%, anatase) is mixed with 91 mL of a NaOH (Fisher, ACS certified, 99%) aqueous solution (10 M). The mixed solution is then sealed in a 130 mL Teflon-lined stainless steel autoclave and stirred at temperatures ranging from 150 to 240 °C for 24 h to obtain $Na_2Ti_3O_7$ with different aspect ratios. Following this reaction, the resultant

Received: November 9, 2013
Accepted: March 26, 2014
Published: March 26, 2014

   dx.doi.org/10.1021/am405038r | *ACS Appl. Mater. Interfaces* 2014, 6, 5450−5455

$Na_2Ti_3O_7$ NWs were soaked in an aqueous 0.2 M hydrochloric acid (Fisher, 37%) solution for 4 h to produce hydrogen titanate ($H_2Ti_3O_7$) NWs. The $H_2Ti_3O_7$ NWs were then washed using repeated centrifugation from DI water with vortex mixing used to redisperse the NWs between each wash, until the pH reached around 7 with subsequent drying at 60 °C for 12 h.

$BaTiO_3$ NWs were subsequently synthesized through a second hydrothermal reaction to convert the $H_2Ti_3O_7$ NWs of varying aspect ratio using a $Ba(OH)_2{\cdot}8H_2O$ (Sigma-Aldrich, ACS certified, 98%) aqueous solution. First, the obtained NW powder was dispersed in 140 mL of a 0.05 M $Ba(OH)_2{\cdot}8H_2O$ solution, using a molar ratio Ba:Ti = 2:1 to fully transfer the $H_2Ti_3O_7$ NWs to $BaTiO_3$ NWs. The solution was then sonicated for 5 min and saturated with nitrogen. The final mixture was transferred into a 200 mL Teflon lined stainless steel reactor and kept at 210 °C for 85 min. The resulting NWs was briefly soaked into a 0.2 M HCl aqueous solution and then washed with DI water and ethanol (Fisher undenatured) to obtain $BaTiO_3$ NWs.

2.2. Preparation of Nanocomposites. To help the $BaTiO_3$ NWs have a homogeneous dispersion in PVDF matrix, the obtained NWs were functionalized by ethylenediamine. The functionalization was carried out by mixing the $BaTiO_3$ powder with ethylenediamine followed by vortex mixing for 5 min then sonicating for 1 h, following by heated the solution to 90 °C in a water bath for 1 h. The precipitate was collected by centrifugation with subsequent drying at 70 °C under vacuum for 12 h.

The nanocomposite films were prepared by mixing $BaTiO_3$ NWs into a solution of 7 wt % PVDF in dimethylformamide (DMF) by sonication for 2 h. The solution was then cast onto a ceramic glass plate to form thin films at 90 °C in the vacuum oven. To reduce the thickness and produce smooth void-free films, the films (approximately 40 mm × 20 mm × 0.5 mm) were hot pressed at 170 °C for 1 h to yield a final film with thickness of approximately 0.1 mm. Finally, gold (approximately 10 nm) was sputtered onto both side of the film to serve as electrodes for dielectric measurement.

2.3. Characterization. The morphology of the nanowires and nanocomposites were characterized by scanning electron microscopy (FE-SEM; 6335F, JEOL). The crystalline structure of the NWs were determined by an X-ray diffractometer (XRD, CPS, 120) with Cu Kα source. To characterize the functionalization of the nanowires, Fourier-transform infrared spectroscopy (FTIR) was performed by a FTIR spectrometer (6700, Nicolet) with a Smart Orbit ATR accessory. The film thickness is measured by Mitutoyo Micrometer with 0.001 mm resolution. The dielectric constant of the nanocomposite films was calculated from the capacitance measured by an LCR meter (4284A, Agilent) at 1 kHz at 1 V_{rms} with a parallel equivalent circuit.[8]

RESULTS AND DISCUSSION

The two-step hydrothermal reaction is employed to achieve a large-scale and highly efficient synthesis of $BaTiO_3$ NWs. The first hydrothermal reaction is used to synthesis hydrogen titanate NWs because of its extensive research history and easily controlled nanowire morphology.[20,22,23] More importantly, hydrogen titanate is a layered titanate, which is a good precursor for soft chemical synthesis because of its open structure fit for ion exchange properties.[22,24] To adjust the aspect ratio of the hydrogen titanate NWs, we changed the hydrothermal temperature from 150 to 240 °C. Figure 1 shows the SEM images of the free-standing hydrogen titanate NWs synthesized at different temperatures. With an increase in temperature, the length of the NWs is increased much greater compared to the diameter, resulting in a higher AR. The structure of the hydrogen titantate ($H_2Ti_3O_7$) was determined by XRD as shown in Figure 2.

The $BaTiO_3$ NWs were synthesized from the $H_2Ti_3O_7$ NWs by a second hydrothermal reaction in aqueous $Ba(OH)_2{\cdot}8H_2O$ solution. The second hydrothermal process was designed to transfer the hydrogen titanate to barium titanate and specifically

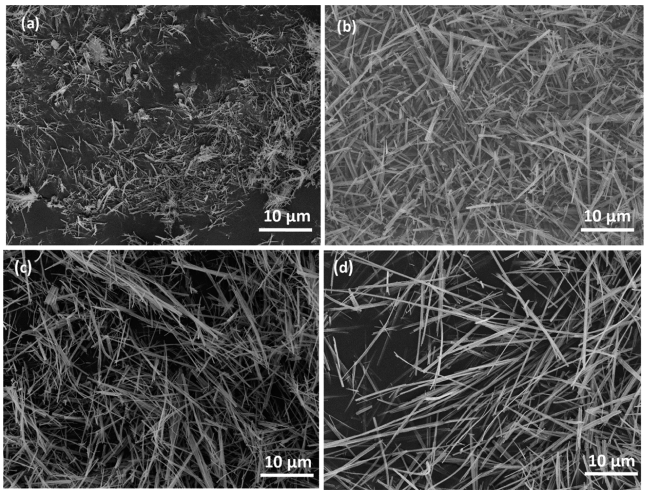

Figure 1. SEM images of hydrogen titanate NWs prepared at different temperatures: (A) 150, (B) 180, (C) 200, and (D) 240 °C.

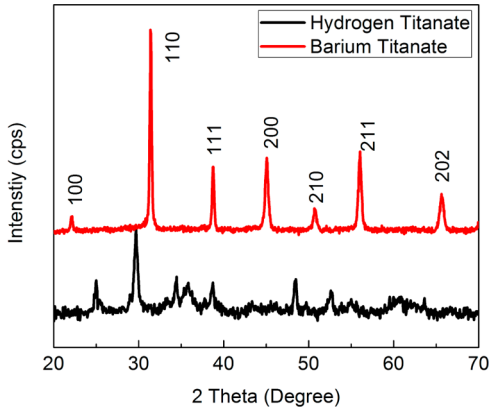

Figure 2. XRD patterns of hydrogen titanate ($H_2Ti_3O_7$) synthesized at 240 °C in the first hydrothermal reaction and corresponding barium titante ($BaTiO_3$) NWs obtained in the second hydrothermal reaction.

retain the morphology of the nanowires as shown in Figures 2 and 3. The diffraction pattern (Figure 2) can be assigned to the $BaTiO_3$ crystal structure (JCPDS, 81−2203) without any

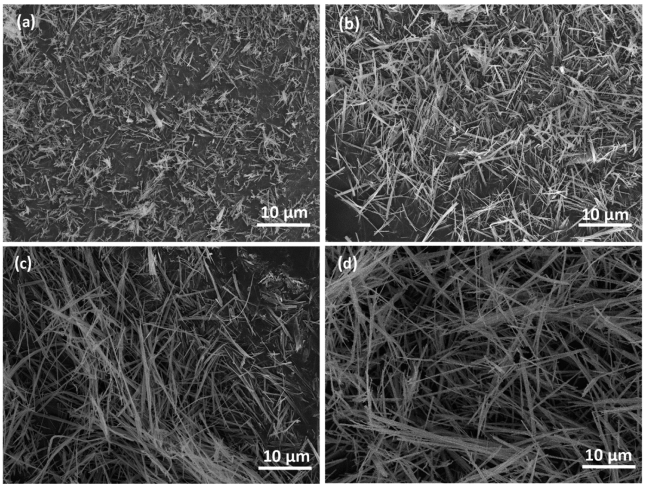

Figure 3. SEM images of $BaTiO_3$ NWs at different temperature: (a) 150, (b) 180, (c) 200, and (d) 240 °C.

dx.doi.org/10.1021/am405038r | ACS Appl. Mater. Interfaces 2014, 6, 5450−5455

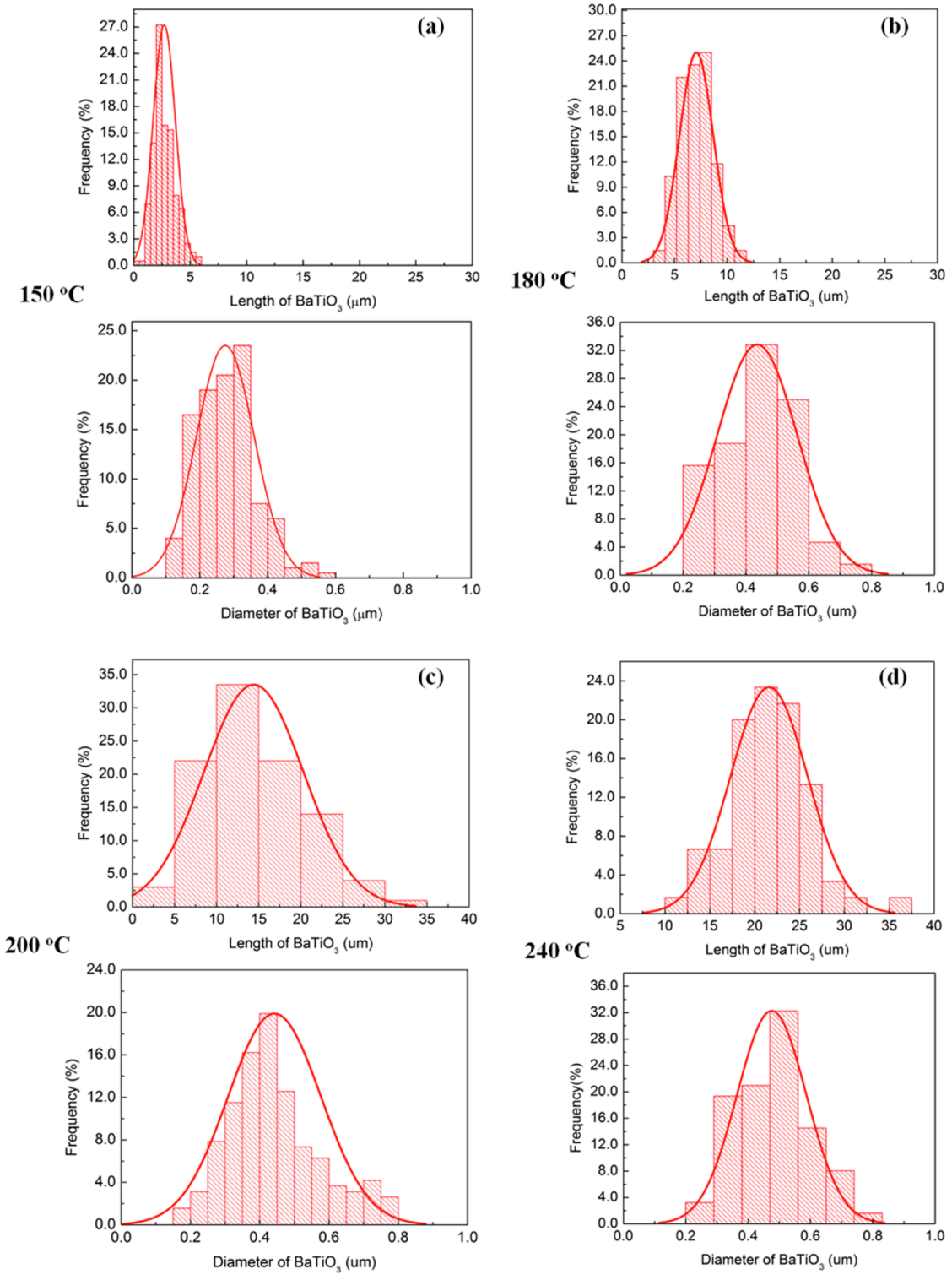

Figure 4. $BaTiO_3$ particle size distribution dependent on the hydrothermal temperature: (a) 150, (b) 180, (c) 200, and (d) 240 °C.

indication of crystalline byproducts such as $BaCO_3$ or TiO_2. Figure 3 shows the free-standing $BaTiO_3$ NWs after second hydrothermal transformation from the precursor hydrogen titanate. It is clearly demonstrated that the aspect ratio of $BaTiO_3$ NWs increases with increasing hydrothermal temperature of the hydrogen titanate. In addition, it should be mentioned that the morphology of the $BaTiO_3$ highly depend on the second hydrothermal conditions, such as nature of the precursors, reaction duration and temperature. Previously, it has demonstrated various morphology of $BaTiO_3$ are yield at the second hydrothermal transformation, such as cubic, starfish-like, and snowflake-like.[20] The $BaTiO_3$ NWs are successfully prepared here by employing high transformation temperature and short reaction time. The length and diameter of the $BaTiO_3$ wire were analyzed using SEM images through ImageJ software as shown in Figure 4. It clearly shows that with an increase in temperature, the length of the NWs is increased much greater compared to the diameter, resulting in a higher

dx.doi.org/10.1021/am405038r | ACS Appl. Mater. Interfaces 2014, 6, 5450−5455

AR. The aspect ratio distribution of $BaTiO_3$ NWs calculated from Figure 4 is summarized in Figure 5. It clearly shows that

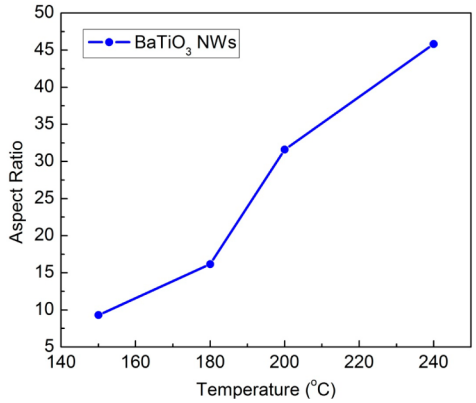

Figure 5. Aspect ratio of $BaTiO_3$ NWs dependent on the hydrothermal reaction temperature.

the aspect ratio of the $BaTiO_3$ NWs highly depend on the hydrothermal temperature. The aspect ratio is increased with increasing temperature from 9.5 to 45.8 corresponding to 150 and 240 °C, respectively.

To increase compatibility and improve dispersion of the fillers in the matrix, the $BaTiO_3$ NWs were surface functionalized by ethylenediamine. The modified $BaTiO_3$ powder was subsequent dried at 70 °C under vacuum for 12 h in the experiment. Therefore, the simple adsorption of the molecule will be removed at 70 °C under vacuum for 12 h due to the evaporation of ehylenediamine residue. The surfaces of $BaTiO_3$ NWs before and after the modification with ethylenediamine were characterized by FTIR as shown in Figure 6a. It can be observed the binding of amine groups around 1450 cm^{-1},[25] which can be acted as a bridge to bind $BaTiO_3$ with the PVDF matrix as shown in the inset of Figure 6a. Figure 6b shows the top surface of the nanocomposite with 10 vol % $BaTiO_3$ NWs. It indicates that the functionalized fillers with amine groups have been homogeneously dispersed in the PVDF matrix without voids in the film.[26]

The dielectric constant of the nanocomposites was measured with an Agilent 4980A LCR meter at a frequency of 1 kHz. The dependency of the nanocomposite dielectric constant on the concentration and aspect ratio of the fillers is shown in Figure 7. The dielectric constant of the nanocomposites increases with increasing volume fraction of the fillers due to the higher dielectric permittivity of $BaTiO_3$ as compared with the neat PVDF polymer (9.8 at 1 kHz). It is clearly demonstrated that the dielectric constant of the nanocomposite can be significantly improved by increasing the aspect ratio of $BaTiO_3$ NWs, while the loss tangent shows little variation with value around 0.04 at 1 kHz under different of aspect ratio and volume fraction of $BaTiO_3$ NWs. The loss tangent of PVDF matrix is around 0.06 at 1 kHz, which indicates that incorporation of $BaTiO_3$ NWs decrease the loss tangent of the film. It should be noted that the dielectric constant of the nanocomposite with 30 vol % $BaTiO_3$ NWs (aspect ratio 45.8) can reach a dielectric constant as high as 44.3, which is 30.7% higher than samples with a low aspect ratio (9.3) and 352% larger than the polymer matrix. This technique efficiently improves the dielectric property of the nanocomposites without the need for additional fillers.

This study has determined the relation between the aspect ratio of fillers and dielectric constant of the nanocomposites. It shows that the dielectric constant of the nanocomposites can be improved by higher aspect ratio fillers. This finding as well as the previous research demonstrates that the aspect ratio plays a critical role in defining the dielectric constant of the nanocomposites compared to the size effect.[8] There are many theoretical models that have shown the improved dielectric constant by using high aspect ratio fillers.[13−15,27] For example, the aspect ratio effect can be described by the Maxwell−Garnet model[15,27]

$$\varepsilon = \varepsilon_2 + \varepsilon_2 \frac{\frac{\emptyset_1}{3}\sum_{i=x,y,z}\frac{\varepsilon_1-\varepsilon_2}{\varepsilon_2+N_i(\varepsilon_1-\varepsilon_2)}}{1-\frac{\emptyset_1}{3}\sum_{i=x,y,z}\frac{N_i(\varepsilon_1-\varepsilon_2)}{\varepsilon_2+N_i(\varepsilon_1-\varepsilon_2)}}$$

where N_i is known as the depolarization factor of ellipsoids in the x, y, z direction. For the NWs morphology in the experiment, where the radii $a_x > a_y = a_z$, N_i can be expressed as following

$$N_i = \left(\frac{\ln(1+e)}{1-e} - 2e\right)(1-e^2)/2e^3$$

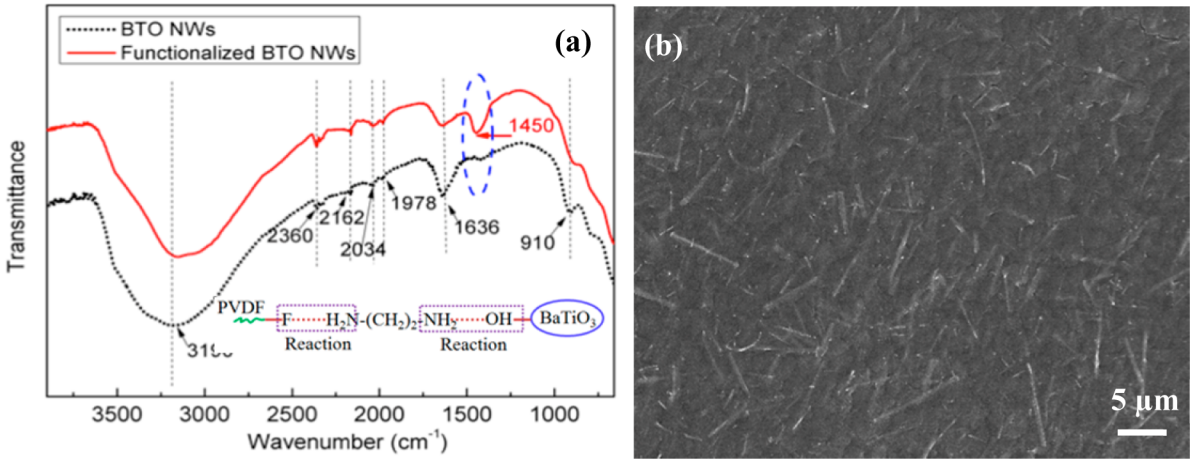

Figure 6. (a) FTIR spectra of $BaTiO_3$ NWs and modified $BaTiO_3$ NWs by ethylenediamine. (b) SEM topography of the nanocomposites with 10% $BaTiO_3$ NWs.

dx.doi.org/10.1021/am405038r | ACS Appl. Mater. Interfaces 2014, 6, 5450−5455

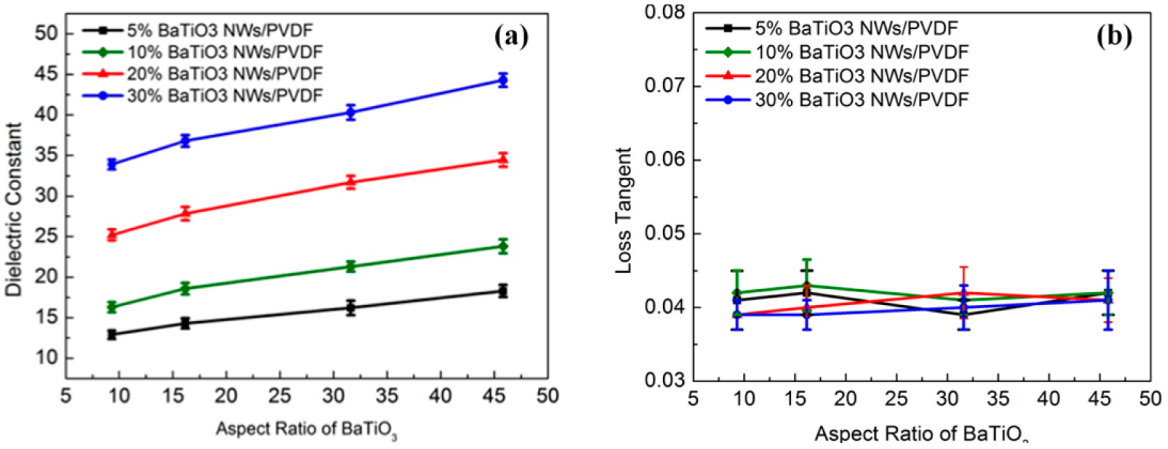

Figure 7. (a) Dielectric constant and (b) loss tangent of the nanocomposites measured at 1 kHz as a function of aspect ratio and volume fraction of $BaTiO_3$ NWs.

$$e = \sqrt{1 - a_y^2/a_x^2}$$

The Maxwell–Garnet model demonstrates that the dielectric permittivity of composite is improved by high aspect ratio filler.[18,27] Andrews et al. also developed finite element and micromechanics models to investigate the effect of aspect ratio on the dielectric performance of the composites, and it is demonstrated that the higher aspect ratio NWs will improve the dielectric permittivity of the nanocomposites.[13] The benefits of using high aspect ratio fillers can be also explained through the following aspects. First, the high-aspect-ratio fillers reach the percolation threshold easier than the low aspect ratio nanowires, which allows connectivity or continuous passage in the system and improves the dielectric properties of the nanocomposites.[28,29] Additionally, the high-aspect-ratio nanowires can improve the dielectric constant of the composites due to the large dipole moment.[30] Finally, Brunauer–Emmer–Teller (BET) surface area analysis has also demonstrated that the high-aspect-ratio fillers have lower surface area than low aspect ratio fillers, which helps reduce the surface energy, thus preventing agglomeration in the nanocomposites. All these aspects work to make high-aspect-ratio nanowires more effective in enhancing the dielectric constant of the nanocomposites.

3. CONCLUSION

In summary, we have reported a novel and simple method to control the aspect ratio of $BaTiO_3$ NWs by changing the hydrothermal reaction temperature. The aspect ratio of the nanowires can reach as high as 45.8. The relationship between the dielectric constant of the nanocomposites and the aspect ratio fillers is the first time to be quantified with focusing on high aspect ratio. It is demonstrated that the dielectric constant of the nanocomposite can be highly efficiently improved by the high aspect ratio of the fillers without additional fillers or defect incorporation into the nanocomposites. This study can potentially be used to develop high-κ nanocomposites for various electric applications.

AUTHOR INFORMATION

Corresponding Author

*E-mail: hsodano@ufl.edu.

Author Contributions

The manuscript was written through contributions of all authors. All authors have given approval to the final version of the manuscript.

Notes

The authors declare no competing financial interest.

ACKNOWLEDGMENTS

The authors gratefully acknowledge the support from the National Science Foundation (Grant CMMI-0826159) and the Arkema Inc. for providing the PVDF used for this work.

REFERENCES

(1) Li, Y.; Huang, X.; Hu, Z.; Jiang, P.; Li, S.; Tanaka, T. *ACS Appl. Mater. Interfaces* **2011**, *3*, 4396–4403.
(2) Zirkl, M.; Haase, A.; Fian, A.; Schön, H.; Sommer, C.; Jakopic, G.; Leising, G.; Stadlober, B.; Graz, I.; Gaar, N.; Schwödiauer, R.; Bauer-Gogonea, S.; Bauer, S. *Adv. Mater.* **2007**, *17*, 2241–2245.
(3) Tang, H.; Sodano, H. A. *Nano Lett.* **2013**, *13*, 1373–1379.
(4) Ávila, H. A.; Ramajo, L. A.; Góes, M. S.; Reboredo, M. M.; Castro, M. S.; Parra, R. *ACS Appl. Mater. Interfaces* **2013**, *5*, 505–510.
(5) Tang, H.; Lin, Y.; Sodano, H. A. *Adv. Energy Mater.* **2012**, *4*, 469–476.
(6) Tomer, V.; Manias, E.; Randall, C. A. *J. Appl. Phys.* **2011**, *4*, 044107.
(7) Kim, P.; Jones, S. C.; Hotchkiss, P. J.; Haddock, J. N.; Kippelen, B.; Marder, S. R.; Perry, J. W. *Adv. Mater.* **2007**, *7*, 1001–1005.
(8) Tang, H.; Lin, Y.; Andrew, C.; Sodano, H. A. *Nanotechnology* **2011**, *22*, 015702.
(9) Li, J.; Khanchaitit, P.; Han, K.; Wang, Q. *Chem. Mater.* **2010**, *18*, 5350–5357.
(10) Li, J.; Seok, S.; Chu, B.; Dogan, F.; Zhang, Q.; Wang, Q. *Adv. Mater.* **2009**, *2*, 217–221.
(11) Li, J.; Claude, J.; Norena-Franco, L.; Seok, S. W.; Q. *Chem. Mater.* **2008**, *20*, 6304–6306.
(12) Kim, P.; Doss, N. M.; Tillotson, J. P.; Hotchkiss, P. J.; Pan, M. J.; Marder, S. R.; Li, J.; Calame, J. P.; Perry, J. W. *ACS Nano* **2009**, *9*, 2581–2592.
(13) Andrews, C.; Lin, Y.; Sodano, H. A. *Smart Mater. Struct.* **2010**, *2*, 025018.
(14) Patil, S. K.; Koledintseva, M. Y.; Schwartz, R. W.; Huebner, W. *J. Appl. Phys.* **2008**, *7*, 074108.
(15) Sihvola, A. H.; Alanen, E. *IEEE Trans. Geosci. Remote. Sens.* **1991**, *4*, 679–687.
(16) Tang, H.; Lin, Y.; Sodano, H. A. *Adv. Energy Mater.* **2013**, *3*, 451–456.

(17) van den Ende, D. A.; van Kempen, S. E.; Wu, X.; Groen, W. A.; Randall, C. A.; van der Zwaag, S. *J. Appl. Phys.* **2012**, *12*, 124107.
(18) Wang, Z.; Nelson, J. K.; Miao, J.; Linhardt, R. J.; Schadler, L. S.; Hillborg, H.; Zhao, S. *IEEE Trans. Dielectr. Electr. Insul.* **2012**, *3*, 960−967.
(19) Song, Y.; Shen, Y.; Liu, H.; Lin, Y.; Li, M.; Nan, C. *J. Mater. Chem.* **2012**, *16*, 8063−8068.
(20) Bao, N.; Shen, L.; Srinivasan, G.; Yanagisawa, K.; Gupta, A. *J. Phys. Chem. C* **2008**, *23*, 8634−8642.
(21) Zhang, Y. X.; Li, G. H.; Jin, Y. X.; Zhang, Y.; Zhang, J.; Zhang, L. D. *Chem. Phys. Lett.* **2002**, *3*−*4*, 300−304.
(22) Buscaglia, T. M.; Harnagea, C.; Dapiaggi, M.; Buscaglia, V.; Pignolet, A.; Nanni, P. *Chem. Mater.* **2009**, *21*, 5058−5065.
(23) Kang, S.; Jang, H.; Kim, K.; Park, B. H.; Jung, M.; Kim, Y. *Mater. Res. Bull.* **2008**, *4*, 996−1003.
(24) Jiang, C.; Kiyofumi, K.; Wang, Y.; Koumoto, K. *Cryst. Growth Des.* **2007**, *12*, 2713−2715.
(25) Chandra, S.; Das, P.; Bag, S.; Laha, D.; Pramanik, P. *Nanoscale* **2011**, *4*, 1533−1540.
(26) Dang, Z.; Wang, H.; Xu, H. *Appl. Phys. Lett.* **2006**, *11*, 112902.
(27) Sihvola, A. H.; Kong, J. A. *IEEE Trans. Geosci. Remote. Sens.* **1988**, *26*, 420−429.
(28) McLachlan, D. S.; Blaszkiewicz, M.; Newnham, R. E. *J. Am. Ceram. Soc.* **1990**, *8*, 2187−2203.
(29) Yi, J. Y.; Choi, G. M. *J. Electroceram.* **1999**, *4*, 361−369.
(30) Guo, N. D.; Dibenedetto, S. A.; Tewari, P.; Lanagan, M. T.; Ratner, M. A.; Marks, T. J. *Chem. Mater.* **2010**, *4*, 1567−1578.